frontiers | Frontiers in Materials

TYPE Original Research
PUBLISHED 14 February 2025
DOI 10.3389/fmats.2025.1531950

OPEN ACCESS

EDITED BY
K. H. Leong,
University of Adelaide, Australia

REVIEWED BY
Tifeng Jiao,
Yanshan University, China
Leijiao Li,
Changchun University of Science and Technology, China
Xinping Zhang,
Qingdao University of Science and Technology, China

*CORRESPONDENCE
Yan Zhou,
yzhou1992@ciac.ac.cn
Xiong Zhengrong,
zrxiong@ciac.ac.cn
Xianghai Jing,
aerosun@aliyun.com

RECEIVED 21 November 2024
ACCEPTED 13 January 2025
PUBLISHED 14 February 2025

CITATION
Fu L, Hu J, Luo P, Xiang D, Hui W, Cheng L, Zhou Y, Zhengrong X, Yao D and Jing X (2025) Fabrication and performance of the wide-band highly shielded polyvinylidene fluoride film.
Front. Mater. 12:1531950.
doi: 10.3389/fmats.2025.1531950

Fabrication and performance of the wide-band highly shielded polyvinylidene fluoride film

Liwu Fu[1], Jiangfeng Hu[2], Peng Luo[3], Dong Xiang[2], Wenying Hui[4], Lei Cheng[2], Yan Zhou[5]*, Xiong Zhengrong[5]*, Dengzun Yao[6] and Xianghai Jing[7]*

[1]Pipe China Storage and Transportation Technology Company, Tianjin, China, [2]Pipe China West Pipeline Company, Urumqi, China, [3]Production Department of Pipe China, Beijing, China, [4]Pipe China Gansu Pipeline Company, Lanzhou, China, [5]CAS Key Laboratory of High-Performance Synthetic Rubber and its Composite Materials, Changchun Institute of Applied Chemistry, Chinese Academy of Sciences, Changchun, China, [6]China Special Equipment Inspection and Research Institute, Beijing, China, [7]Lianyungang Jingwei Composite New Materials Co., Ltd., Liangyungang, China

The white weathering layer materials that can effectively block the entire solar light band is of great importance for improving the service life, safety, and reliability of the materials. In this work, $CsxWO_3$@PDA was prepared by *in situ* polymerization to achieve high absorption in the full spectral range and increase the compatibility between $CsxWO_3$ particles and polyvinylidene fluoride (PVDF). PVDF composite films with different particle contents were prepared through compounding with titanium dioxide (TiO_2) and $CsxWO_3$@PDA. The prepared composite films were characterized by FT-IR, field emission scanning electron microscopy, universal material testing machine, whiteness meter, and ultraviolet visible spectroscopy. The results showed that the CsPVDF composite films with $CsxWO_3$@PDA and TiO_2 exhibited a whiteness level higher than 74, a transmittance of less than 5% in the wavelength range of 200–2500 nm, and a transmittance close to zero in the range below 1750 nm, demonstrating excellent shielding effect. The xenon lamp aging test also confirmed that the composite films had excellent weather resistance after aging 500 h. At the same time, adding a certain amount of $CsxWO_3$@PDA could improve the tensile strength of PVDF.

KEYWORDS

opaque film, titanium dioxide, PVDF, CsxWO3@PDA, wide-band shielded

1 Introduction

The importance of lightweight, high-performance materials across multiple industries is increasing with the rapid advancement of technology. These materials play crucial roles in fields such as aerospace, construction, transportation, and energy (Mountasir et al., 2015; Lv et al., 2022). They can not only enhance the performance of structures but also expand the boundaries of design, enabling the realization of more efficient and sustainable solutions (Ali and Andriyana, 2020; Jiang et al., 2016). Flexible fiber-reinforced composite materials, a specialized class of lightweight materials with a multi-layer structure, are widely utilized in applications such as aerostats, flexible structures, and inflatable construction. The lightweight and high-strength properties of these materials render them ideal candidates for the implementation of high-performance structures (Kang et al., 2006; Meng et al., 2017). The properties of flexible fiber-reinforced

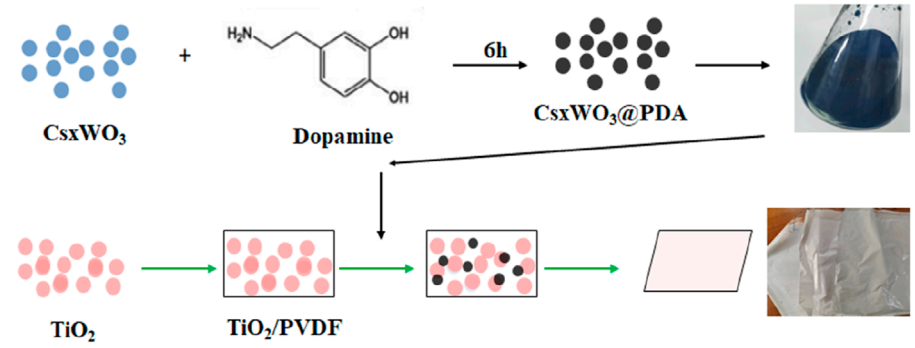

FIGURE 1
Fabrication process of PVDF composite films.

TABLE 1 Composition of samples.

Sample	Weight percentage			
	PVDF	TiO_2	CsxWO$_3$@PDA	CsxWO$_3$
CPVDF-1	80.0%	19.9%	0.1%	0.0%
CPVDF-2	80.0%	19.5%	0.5%	0.0%
CPVDF-3	80.0%	19.0%	1.0%	0.0%
CPVDF-4	80.0%	18.0%	2.0%	0.0%
TPVDF	80.0%	20.0%	0.0%	0.0%
CsPVDF	80.0%	18.0%	0.0%	2.0%

durability, weatherability, and adaptability to environmental changes, directly influence the reliability and service life of the entire structure. In aerospace, the lightweight and high-strength properties of flexible fiber-reinforced composite materials are critical for increasing the floating height and payload of aerostats (Meng et al., 2016). In architecture, they provide designers with the capability to create flexible, deformable spaces. Furthermore, the applications of flexible fiber-reinforced composite materials are also expanding in the transportation and energy sectors, such as movable structures and temporary facilities. To meet these diverse application requirements, flexible fiber-reinforced composite materials are generally composed of a lightweight and high-strength polymer multilayer, in which the structures are weather-resistant layer/barrier layer/intermediate layer/load-bearing fabric/heat sealing layer from the exterior to the interior. Among these, the weather-resistant layer, as an extremely important functional layer in the composite material, is usually white and directly related to the safety and stability of the aerostats (Lv et al., 2021).

Fluoropolymers are utilized in a wide range of fields due to their excellent weathering and chemical resistance (Améduri, 2023; Puts et al., 2019). The Tedlar, PVF series of composite films of DuPont's are well known for their excellent effective aging resistance with its polyvinyl fluoride as the base resin and inorganic fillers with UV-visible light-blocking capabilities in the current market (Kim et al., 2012). However, there are processing challenges for polyvinyl fluoride due to its insolubility in most solvents and has a decomposition temperature similar to the melting temperature, limiting some of the applications (Alaaeddin et al., 2019). In contrast, polyvinylidene fluoride (PVDF) exhibits favorable aging resistance, abrasion resistance, and excellent mechanical properties (Dallaev et al., 2022). The processing performance of PVDF is also superior. However, it is inherently transparent, with high transmittance to UV and visible light, and cannot be utilized as a weathering layer to protect inner layers from radiation (Liu et al., 2020; Dong et al., 2018). To achieve a high shielding effect in the broad band, researchers have investigated various methods, such as blocking UV light by incorporating UV absorbers such as TiO_2 and benzophenone into the weathering layer (Deng et al., 2019; Jiang et al., 2021). Nevertheless, the shielding performance of these materials usually refers to the visible light region, and the covering ability for the near-infrared light region is even less effective (Muzata et al., 2023; Wu et al., 2019; Silva et al., 2023). Li et al. improved the opacity of PVDF composite films by adding TiO_2 and an extremely small amount of carbon black (Li et al., 2016). However, there was no information about the solar shielding properties. Although the carbon-based nanofiller and metal oxide (such as CuS) could also serve as light-shielding agents through reasonable regulation (Huang and Ruan, 2017; Yang et al., 2024; Yuan et al., 2020; Xu et al., 2017), the strong absorbance of sunlight and the complex preparation process of metal oxide, as well as the high cost, limit the applications in the fields such as aerostat and pneumatic architecture, which needs the materials with high whiteness and low transmittance as much as possible. Therefore, the development of white weathering layer materials that can effectively block the entire solar light band is of great importance for improving the service life, safety, and reliability of the materials. In this regard, novel materials and technologies are being explored. Among them, cesium tungsten bronze powder (Cs_xWO_3) has garnered considerable attention as an energy-saving coating additive, which can absorb more than 90% of near-infrared (NIR) light but not affect the performance in the visible light region (Nakakura et al., 2024; Nakakura et al., 2019; Zhang et al., 2024). Enhanced sunlight shielding can be achieved by compounding it with TiO_2. However,

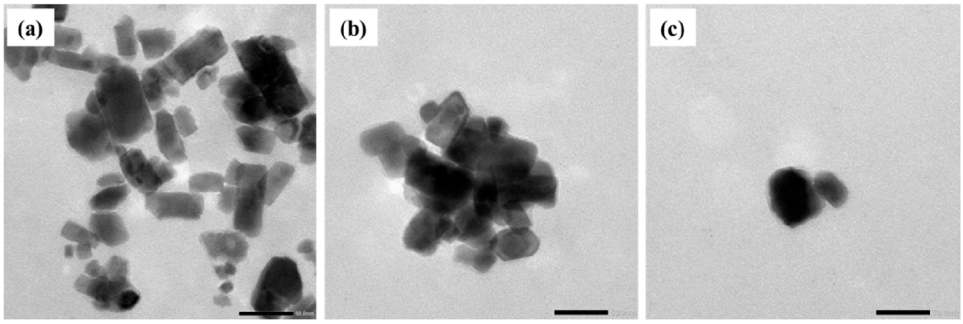

FIGURE 2
TEM images of **(A)** $CsxWO_3$ and **(B, C)** $CsxWO_3$@PDA; the scale bar is 50 nm.

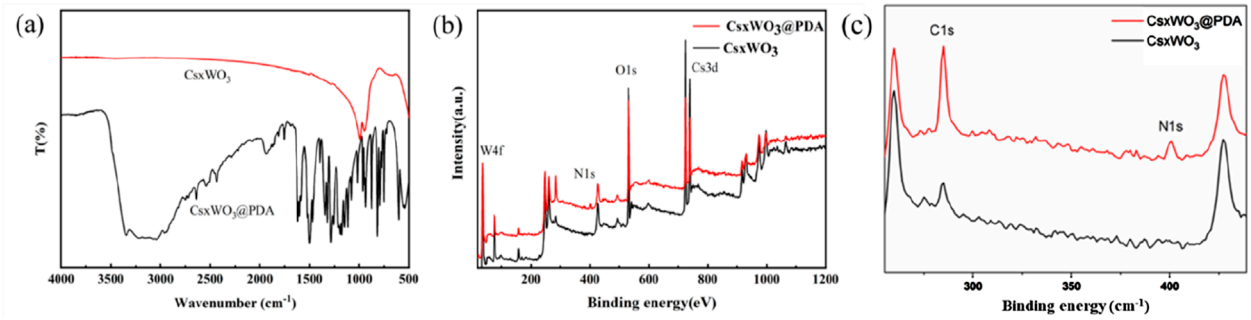

FIGURE 3
(A) FT-IR and **(B, C)** XPS spectra of $CsxWO_3$ and $CsxWO_3$@PDA particles.

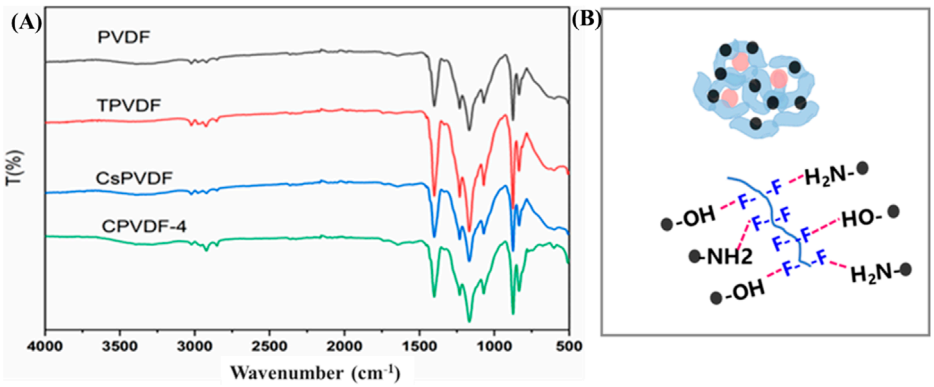

FIGURE 4
(A) FT-IR spectra of PVDF composite films and **(B)** hydrogen bonding among PVDF and $CsxWO_3$@PDA.

there is still a challenge for the dispersion of Cs_xWO_3 in the resin matrix.

Thus, in this study, dopamine, which is compatible with the resin, was utilized to modify Cs_xWO_3 through coating and compounded with TiO_2 to achieve effective shielding in broad wavelength bands and improved mechanical properties. This research can provide insights for the design of weathering layers for aerostat envelope materials and inflatable building materials.

2 Experimental section

2.1 Materials

Rutile TiO_2 with an average particle size of approximately 300 nm and $CsxWO_3$ with an average particle size of approximately 30 nm were supplied by DuPont's and Yingcheng New Materials Co., Ltd., respectively. Dopamine hydrochloride with a purity of

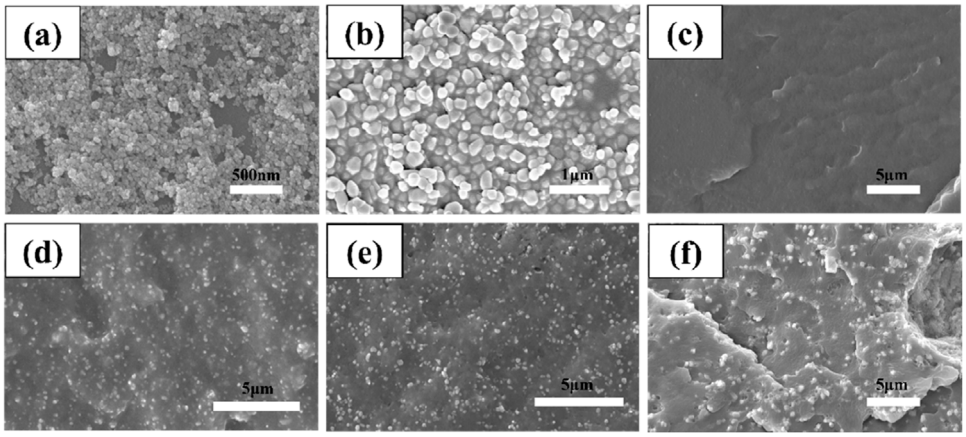

FIGURE 5
SEM images of **(A)** $CsxWO_3$@PDA, **(B)** TiO_2, **(C)** PVDF, **(D)** TPVDF, **(E)** CPVDF-4, and **(F)** CsPVDF.

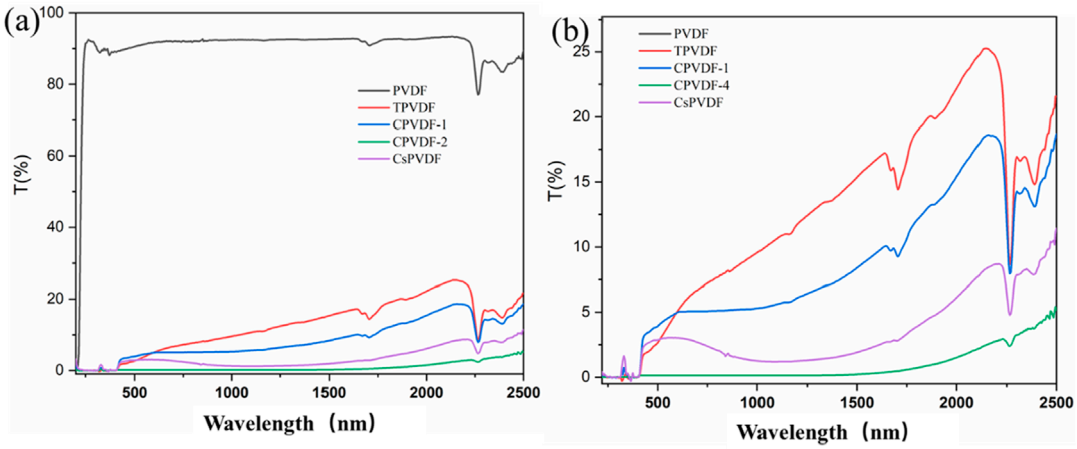

FIGURE 6
UV-Vis-NIR transmission spectra **(A)** and amplified spectra **(B)** of PVDF composite films.

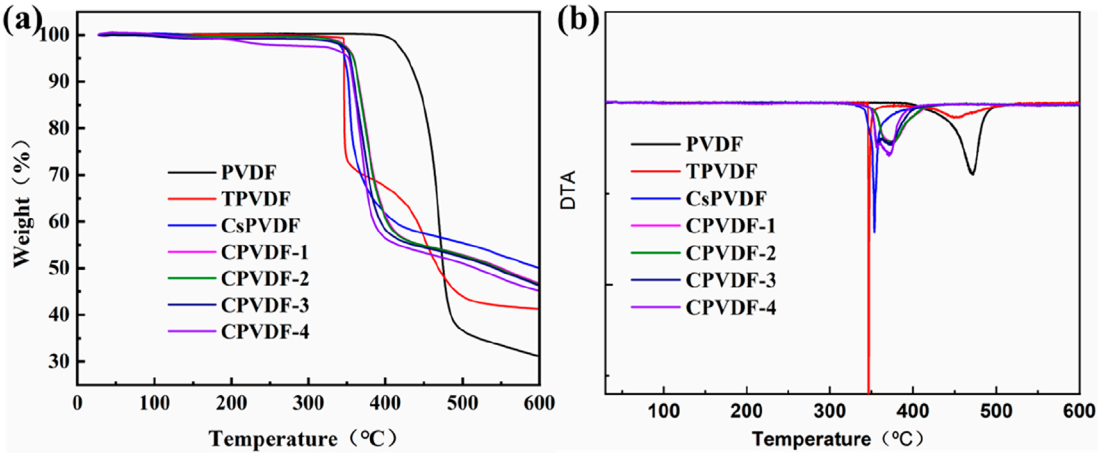

FIGURE 7
(A) TGA and **(B)** DTA curves of PVDF composite films.

TABLE 2 TGA data on $CsxWO_3$@PDA/PVDF in nitrogen.

Sample	Temperature at 5% weight loss (°C)	Temperature at 10% weight loss (°C)	Temperature at maximum weight loss rate (°C)
PVDF	428.1	441.1	472.2
TPVDF	342.2	346.3	347.7
CsPVDF	346.9	351.7	353.3
CPVDF-1	358.6	365.1	373.5
CPVDF-2	358.1	364.4	373.1
CPVDF-3	354.2	358.9	372.5
CPVDF-4	351.8	357.5	372.4

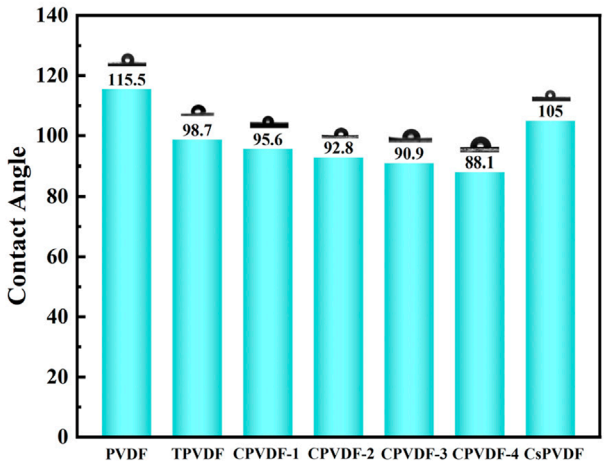

FIGURE 8
Water contact angle of the PVDF composite films.

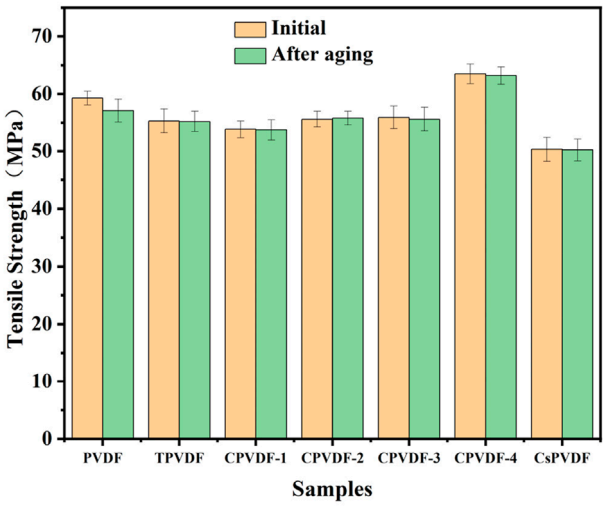

FIGURE 9
Comparison of the fracture strength of PVDF films before and after aging.

98% and tris(hydroxymethyl)aminomethane solution (Tris) with a purity ≥99.9% were purchased from Energy Chemical and Aladdin Reagent Co., Ltd., respectively. The PVDF (SolefVR 6010) resin was obtained from Solvay Solexis Co., Ltd. N′, N′-dimethylformamide (DMF) was brought from Beijing Chemical Factory.

2.2 Preparation of $CsxWO_3$@PDA

As shown in Figure 1, 0.5 g/L $CsxWO_3$ dispersion was obtained first under the assistance of a cell disruptor. Then, a certain amount of dopamine hydrochloride was added and stirred to dissolve. Subsequently, a measured amount of the Tris buffer solution was mixed into the above dispersion to adjust the *pH* of the system to 8.5. Finally, the dispersion was washed and centrifuged with deionized water for 6 10 times after reacting 6 h at room temperature to obtain $CsxWO_3$@PDA particles, which were dried for later use.

2.3 Preparation of the $CsxWO_3$@PDA/PVDF film

The composite films were prepared by solution casting. Initially, the PVDF solution with the fraction of 10.0 wt% and 0.1 g/L $CsxWO_3$@PDA dispersion in DMF were prepared for use. Soon afterward, a certain amount of TiO_2 and $CsxWO_3$@PDA were dispersed into the PVDF solution and stirred at a speed of 1,000 rpm for 2 h at room temperature. Then, the films were fabricated by pouring the suspension onto a glass substrate, which was kept in a horizontal level and coated with a casting stick and dried at 80°C to obtain a film with a thickness of approximately 50 μm. The samples were named in sequence as CPVDF-1, CPVDF-2, CPVDF-3, and CPVDF-4, where the total amount of $CsxWO_3$@PDA and TiO_2 was always controlled at 20.0 wt%. For comparison, samples containing 20.0 wt% TiO_2 and 18.0 wt% TiO_2 +2.0% $CsxWO_3$ were prepared

TABLE 3 Mechanical properties of PVDF composite films.

Strength (MPa)	PVDF	TPVDF	CPVDF-1	CPVDF-2	CPVDF-3	CPVDF-4	CsPVDF
Original	59.3 ± 1.2	55.3 ± 2.1	53.8 ± 1.5	55.6 ± 1.4	55.9 ± 2.0	63.5 ± 1.7	53.2 ± 2.1
Aging 500 h	57.1 ± 2.0	55.2 ± 1.8	53.7 ± 1.8	55.8 ± 1.2	55.6 ± 2.1	63.2 ± 1.5	52.9 ± 1.7

and named TPVDF and CsPVDF, respectively. The composition of samples is listed in Table 1.

2.4 Characterization

The structure of $CsxWO_3$@PDA composite particles and composite film was characterized by X-ray photoelectron spectroscopy (XPS, Thermo ESCALAB250 X, Thermo Scientific Company, United States) with Al-Kα radiation and Fourier transform infrared spectroscopy (FT-IR, INVENIO-R, Bruker, Germany) over the wavenumber range of 400–4,000 cm^{-1}.

The morphology of inorganic fillers and the resulting films were characterized using a field-emission scanning electron microscope (FESEM, XL-30, FEI company, United States) with an acceleration voltage of 10 kV and a transmission electron microscope (TEM, JOEL-1400, Japan) under an acceleration voltage of 120 kV, respectively. The cross section of the composite film was obtained by quenching in liquid nitrogen, and the samples were sputter-coated with gold before testing.

Ultraviolet-visible near-infrared absorption performance was evaluated using a UV3600 spectrometer (Shimadzu, Japan) with a scanning interval of 2 nm/s and a scanning range of 200–2,500 nm.

The whiteness test of the material was conducted on a whiteness meter (Lichen, LC-WSB-2Y), which was calibrated using a standard whiteboard, which was the average value calculated of at least five points.

The composite films were cut into dumbbell-shaped strips and placed in a xenon lamp aging chamber for 500 h, followed by testing of mechanical properties at a stretching rate of 200 mm/min. At least 5 strips were tested, and the average value was calculated.

3 Results and discussions

3.1 Structural characterization of $CsxWO_3$@PDA

Figure 2 shows the TEM images of $CsxWO_3$ and $CsxWO_3$@PDA particles. It can be seen that $CsxWO_3$ was in an irregular rectangular shape, and an obvious circle appeared in $CsxWO_3$@PDA, which indicated the successful cladding of PDA.

Figure 3A shows the FT-IR and XPS spectra of $CsxWO_3$ and $CsxWO_3$@PDA particles. It can be seen that after being coated with PDA, the characteristic absorption peaks of the stretching vibrations of phenolic hydroxyl and amine, imine N-H bonds appeared at 3,100–3,600 cm^{-1}. The peak at 1,600 cm^{-1} corresponded to the stretching vibrations of the benzene ring C=C and the bending vibrations of N-H, and the shear vibration peak of N-H appeared at 1,510 cm^{-1}, which also indicated the successful preparation of $CsxWO_3$@PDA. At the same time, for the XPS peaks (Figures 3B, C), a characteristic peak of N1s appeared at 402 eV after being coated with PDA, which also implied the successful synthesis of $CsxWO_3$@PDA composite particles.

3.2 Structural characterization of PVDF composite films

It can be seen from Figure 4 that there was no new characteristic peak appearing after compounding with TiO_2, $CsxWO_3$, or $CsxWO_3$@PDA particles, indicating that there was only a physical interaction between PVDF and the inorganic fillers, and no chemical bonding has occurred. However, the characteristic absorption peaks of CPVDF-4 among 3,300–3,400 cm^{-1} were stronger than those of CsPVDF and TPVDF, which meant there were hydrogen bonds among PVDF and $CsxWO_3$@PDA (Figure 4B). The existence of $-NH_2$ and −OH groups could form strong hydrogen bonding with the F atom in the C-F bond.

3.3 Microscopic morphology of PVDF composite films

Figure 5 shows the morphologies of TiO_2, $CsxWO_3$@PDA, and PVDF composite films. It can be observed from the figure that TiO_2 and $CsxWO_3$@PDA were uniformly distributed in the resin matrix without any significant aggregation. In contrast, obvious aggregation of TiO_2 and $CsxWO_3$ particles was observed in the matrix (Figure 5F). The uniform dispersion was attributed to the modification of PDA, where −OH and $-NH_2$ could form hydrogen bonds with C-F bonds. In addition, $CsxWO_3$@PDA served as a diluent to a certain extent, which spaced the TiO_2 apart, resulting in more evenly dispersion of particles.

3.4 Whiteness and light shielding properties of PVDF composite films

Whiteness was tested to study the influence of $CsxWO_3$ and TiO_2 on the composite film. The whiteness of TPVDF and CsPVDF was 81.4 and 76.2, respectively. With the increase in $CsxWO_3$@PDA, the whiteness of samples decreased from 80.3 to 74.7, owing to the induction of PDA. Even so, the whiteness of CPVDF was still maintained higher than that of carbon-based and commercial Tedlar.

To verify the light-shielding properties of the composite films, ultraviolet-visible near-infrared (UV-Vis-NIR) transmission tests

were conducted, and the results are shown in Figure 6. The PVDF film had a transmittance close to 90% in the wavelength range of 240–2,500 nm. The transmittance of TPVDF with an addition of 20 wt% TiO_2 was close to zero in the wavelength range below 400 nm because of the excellent ultraviolet absorption properties of rutile TiO_2. In the visible and near-infrared regions above 400 nm, the transmittance of TPVDF increased with the increase in wavelength in the range of 400–2,500 nm and reached 25% at approximately 2,100 nm. The transmittance of CPVDF in the wavelength range above 500 nm decreased significantly with the addition of a small amount of $CsxWO_3$@PDA. Among them, CPVDF-4 with 2.0 wt% $CsxWO_3$@PDA had a transmittance of less than 5% throughout the entire spectrum, where the transmittance was close to zero in the range below 1750 nm. It is the multiple absorption of light at the interface of the core-shell structure for $CsxWO_3$@PDA that contributes to the excellent wide-band shielding properties. However, the transmittance across the entire spectrum of CsPVDF with $CsxWO_3$ and TiO_2 was much higher than that of CPVDF-4, especially in the regions of 400–800 nm and 1,500–2,500 nm. This was mainly because that $CsxWO_3$ has superior absorption performance in the 900–1,500-nm region but higher transmittance in the visible light region, which can also confirm that this is the effective combination of $CsxWO_3$ and PDA. Additionally, except for the pure PVDF film, the transmittance of the ultraviolet region for the other samples was close to zero, indicating that the materials had excellent UV shielding capabilities.

3.5 Thermal stability test

Thermal stability is an important property for practical applications, which was tested in a nitrogen atmosphere, and the resulting curves are shown in Figure 7 and Table 2. The initial decomposition temperature and temperature at 5 wt% loss of the pure PVDF membrane were 392.7°C and 428.1°C, respectively. The thermal decomposition temperature reduced for TPVDF with TiO_2 and $CsxWO_3$, whose temperature at 5 wt% loss was 342.2°C and 346.9°C, respectively, which was speculated that addition of fillers may reduce the activation energy for thermal decomposition. With the increase in dopamine-modified $CsxWO_3$, the 5 wt% loss temperature of the composite films gradually decreased with the increase in $CsxWO_3$@PDA from CPVDF-1 to CPVDF-4, which was 358.6°C, 358.1°C, 354.2°C, and 351.8°C, respectively. The reason was that the interface interaction between $CsxWO_3$@PDA and PVDF had changed, which affected the crystallinity of PVDF and thereby affected the thermal stability of the composite films.

3.6 Contact angle measurement

Through the water contact angle experiment, it can be observed that the water contact angle of pure PVDF was 115.5°, showing good hydrophobicity (Figure 8). The TPVDF showed reduced water contact angle to 98.7° due to the polar functional groups such as hydroxyl on TiO_2, which could increase the surface energy and decrease the water contact angle. Owing to the presence of phenolic hydroxyl and amino groups in dopamine of $CsxWO_3$@PDA, the hydrophilicity of CPVDF-1 to CPVDF-4 was enhanced; thus, the water contact angle of the material decreased with the increase in $CsxWO_3$@PDA from 98.7 to 88.1°. In contrast, the addition of the $CsxWO_3$ powder did not significantly increase the surface energy like $CsxWO_3$@PDA. The reduction in the water contact angle is more conducive to adhesive bonding or heat sealing between PVDF composite films with other functional layers, which is vital for laminated structures.

3.7 Aging performance of PVDF composite films

The aging resistance of the material could be assessed by comparing the mechanical properties of PVDF films before and after aging. Furthermore, the results are shown in Figure 9 and Table 3. The mechanical strength of the PVDF film slightly decreased from 59.3 ± 1.2 MPa to 55.3 ± 2.1 MPa after the addition of 20 wt% TiO_2, which may be due to the large addition fraction of TiO_2 and the lack of special surface treatment, resulting in a slightly poor interfacial bonding strength between TiO_2 and PVDF and led to stress concentration under load. The tensile strength of the sample further decreased to 53.2 ± 2.1 MPa after addition of untreated $CsxWO_3$, where $CsxWO_3$ dispersed poorly in the system, leading to stress concentration. Interestingly, on the basis of TPVDF, the fracture strength of the material increased to some extent with the increase in $CsxWO_3$@PDA content, especially when the addition amount is 2.0 wt%, the tensile strength of CPVDF-4 reached 63.5 ± 1.7 MPa, which was 14.8% higher than the pure PVDF of 55.3 ± 1.9 MPa. This was mainly because the coating of PDA contributed to the formation of a good interface transition between $CsxWO_3$ and PVDF through hydrogen bonding, which maximized the reinforcing effect. The strong hydrogen interaction rendered $CsxWO_3$@PDA as physical crosslinkers, which could serve as the dissipative unit to transfer the force to surrounding segments and particles rapidly. At the same time, 2.0 wt% $CsxWO_3$@PDA also acted as a spacer agent to dilute the dispersion of TiO_2 in the matrix and decrease the aggregates, as shown in Figure 4, improving the incompatibility between the matrix and the filler, ultimately making the material's mechanical properties superior to pure PVDF. Moreover, after 500 h of xenon lamp aging, the mechanical properties of the film changed little, indicating that the material has excellent weather resistance.

4 Conclusion

In this work, $CsxWO_3$ was modified by dopamine *in situ* polymerization, and a series of light-shielding PVDF composite films with TiO_2 and $CsxWO_3$@PDA were prepared through solution casting. Results showed that $CsxWO_3$@PDA and TiO_2 synergically achieved the high whiteness level above 74 and an absorption in the full spectral range and increased the compatibility between $CsxWO_3$ and PVDF, where CPVDF-4 with 18.0 wt% TiO_2 and 2.0 wt% $CsxWO_3$@PDA exhibited a transmittance close to zero in the range below 1750 nm, achieving excellent light shielding over a wide spectral range. Correspondingly, the prepared films showed excellent light aging properties, which were no slight changes after 500 h xenon lamp aging. Furthermore, PDA modification improved the interfacial compatibility between nanoparticles and

PVDF, promoted the uniform dispersion of nanoparticles in the matrix, and thereby enhanced the mechanical properties of the composite film, especially the tensile strength reached 63.5 ± 1.7 MPa, which was notably higher than that of pure PVDF. In addition, the hydrophilicity of composite films was enhanced, which could contribute to the adhesive bonding or heat sealing among PVDF composite films with other functional layers.

Data availability statement

The original contributions presented in the study are included in the article/supplementary material; further inquiries can be directed to the corresponding authors.

Author contributions

LF: conceptualization, methodology, and writing–original draft. JH: writing–original draft. PL: writing–original draft. DX: writing–original draft, data curation, and investigation. WH: writing–original draft, methodology, and resources. LC: writing–original draft. YZ: writing–review and editing, conceptualization, and funding acquisition. XZ: writing–review and editing and writing–original draft. DY: resources and writing–review and editing. XJ: writing–original draft.

Funding

The author(s) declare that financial support was received for the research, authorship, and/or publication of this article. Talent Project - Youth Growth Technology Project of Jilin Province (20240602112RC).

Acknowledgments

The authors gratefully acknowledge the financial support from the Talent Project - Youth Growth Technology Project of Jilin Province (20240602112RC).

Conflict of interest

Author LF was employed by Pipe China Storage and Transportation Technology Company. Authors JH, DX, and LC were employed by Pipe China West Pipeline Company. Author PL was employed by the Production Department of Pipe China. Author WH was employed by Pipe China Gansu Pipeline Company. Author XJ was employed by Lianyungang Jingwei Composite New Materials Co., Ltd.

The remaining authors declare that the research was conducted in the absence of any commercial or financial relationships that could be construed as a potential conflict of interest.

The reviewer LL declared a shared affiliation with the authors YZ and XZ at the time of review.

Generative AI statement

The author(s) declare that no Generative AI was used in the creation of this manuscript.

Publisher's note

References

Alaaeddin, M. H., Sapuan, S. M., Zuhri, M. Y. M., Zainudin, E. S., and Al-Oqla, F. M. (2019). Polyvinyl fluoride (PVF); its properties, applications, and manufacturing prospects. *IOP Conf. Ser. Mater. Sci. Eng.* 538, 012010. doi:10.1088/1757-899x/538/1/012010

Ali, A., and Andriyana, A. (2020). Properties of multifunctional composite materials based on nanomaterials: a review. *RSC Adv.* 10, 16390–16403. doi:10.1039/c9ra10594h

Améduri, B. (2023). Fluoropolymers as unique and irreplaceable materials: challenges and future trends in these specific per or poly-fluoroalkyl substances. *Molecules* 28, 7564. doi:10.3390/molecules28227564

Dallaev, R., Pisarenko, T., Sobola, D., Orudzhev, F., Ramazanov, S., and Trčka, T. (2022). Brief review of PVDF properties and applications potential. *Polymers* 14, 4793. doi:10.3390/polym14224793

Deng, Z., Sun, S., Zhou, M., Huang, G., Pang, J., Dang, L., et al. (2019). Revealing ultrafast energy dissipation pathway of nanocrystalline sunscreens oxybenzone and dioxybenzone. *J. Phys. Chem. Lett.* 10, 6499–6503. doi:10.1021/acs.jpclett.9b02592

Dong, L., Liu, X., Xiong, Z., Sheng, D., Zhou, Y., Lin, C., et al. (2018). Design of UV-absorbing PVDF membrane via surface-initiated AGET ATRP. *Appl. Surf. Sci.* 435, 680–686. doi:10.1016/j.apsusc.2017.11.135

Huang, Z., and Ruan, X. (2017). Nanoparticle embedded double-layer coating for daytime radiative cooling. *Int. J. Heat. Mass Tran.* 104, 890–896. doi:10.1016/j.ijheatmasstransfer.2016.08.009

Jiang, L., Gu, B., and Hu, H. (2016). Auxetic composite made with multilayer orthogonal structural reinforcement. *Compos. Struct.* 135, 23–29. doi:10.1016/j.compstruct.2015.08.110

Jiang, Y., Dong, K., An, J., Liang, F., Yi, J., Peng, X., et al. (2021). UV-protective, self-cleaning, and antibacterial nanofiber-based triboelectric nanogenerators for self-powered human motion monitoring. *ACS Appl. Mater. Interfaces* 13 (9), 11205–11214. doi:10.1021/acsami.0c22670

Kang, W., Suh, Y., Woo, K., and Lee, I. (2006). Mechanical property characterization of film-fabric laminate for stratospheric airship envelope. *Compos. Struct.* 75, 151–155. doi:10.1016/j.compstruct.2006.04.060

Kim, Y.-H., Kim, K.-H., Jo, S.-H., Jeon, E.-C., Sohn, J. R., and Parker, D. B. (2012). Comparison of storage stability of odorous VOCs in polyester aluminum and polyvinyl fluoride Tedlar® bags. *Anal. Chim. Acta* 712, 162–167. doi:10.1016/j.aca.2011.11.014

Li, T., Sheng, D., Xiong, Z., Gao, X., Ji, F., and Yang, Y. (2016). Effect of titanium dioxide (TiO_2) distribution and minute amounts of carbon black on the opacity of PVDF based white composite films. *J. Appl. Polym. Sci.*, 43064. doi:10.1002/app.43064

Liu, K., Deng, L., Zhang, T., Shen, K., and Wang, X. (2020). Facile fabrication of environmentally friendly, waterproof, and breathable nanofibrous membranes with high UV-resistant performance by one-step electrospinning. *Ind. Eng. Chem. Res.* 59, 4447–4458. doi:10.1021/acs.iecr.9b05617

Lv, J., Zhang, Y., Gao, H., and Zhang, T. (2021). Influence of processing and external storage conditions on the performance of envelope materials for stratospheric airships. *Adv. Space Res.* 67, 571–582. doi:10.1016/j.asr.2020.10.016

Lv, J., Zhou, Y., Zhang, Y., Nie, Y., and Wang, Q. (2022). Study of performance of aerostat envelope materials on the coast. *Front. Mater.* 9, 992984. doi:10.3389/fmats.2022.992984

Meng, J., Li, P., Ma, G., Du, H., and Lv, M. (2017). Tearing behaviors of flexible fiber-reinforced composites for the stratospheric airship envelope. *Appl. Compos. Mater.* 24, 735–749. doi:10.1007/s10443-016-9539-7

Meng, J., Lv, M., Tan, D., and Li, P. (2016). Mechanical properties of woven fabric composite for stratospheric airship envelope based on stochastic simulation. *J. Reinf. Plast. Compos.* 35, 1434–1443. doi:10.1177/0731684416652947

Mountasir, A., Hoffmann, G., Cherif, C., Löser, M., and Grossmann, K. (2015). Competitive manufacturing of 3D thermoplastic composite panels based on multi-layered woven structures for lightweight engineering. *Compos. Struct.* 133, 415–424. doi:10.1016/j.compstruct.2015.07.071

Muzata, T. S., Gebrekrstos, A., Orasugh, J. T., and Ray, S. S. (2023). An overview of recent advances in polymer composites with improved UV-shielding properties. *J. Appl. Polym. Sci.* 140, e53693. doi:10.1002/app.53693

Nakakura, S., Arif, A. F., Machida, K., Adachi, K., and Ogi, T. (2019). Cationic defect engineering for controlling the infrared absorption of hexagonal cesium tungsten bronze nanoparticles. *Inorg. Chem.* 58, 9101–9107. doi:10.1021/acs.inorgchem.9b00642

Nakakura, S., Machida, K., Inose, M., Wakabayashi, M., Sato, K., and Tsunematsu, H. (2024). Rational cationic disorder in hexagonal cesium tungsten bronze nanoparticles for infrared absorption materials. *Inorg. Chem.* 63, 2486–2494. doi:10.1021/acs.inorgchem.3c03666

Puts, G. J., Crouse, P., and Ameduri, B. M. (2019). Polytetrafluoroethylene: synthesis and characterization of the original extreme polymer. *Chem. Rev.* 119, 1763–1805. doi:10.1021/acs.chemrev.8b00458

Silva, M. R. F., Alves, M. F. R. P., Cunha, J. P. G. Q., Costa, J. L., Silva, C. A., Fernandes, M. H. V., et al. (2023). Nanostructured transparent solutions for UV-shielding: recent developments and future challenges. *Mater. Today Phys.* 35, 101131. doi:10.1016/j.mtphys.2023.101131

Wu, D., Zhou, C., Lu, G., Zhou, Y., and Shen, Y. (2019). Simultaneous membrane fouling mitigation and emerging pollutant benzophenone-3 removal by electro-peroxone process. *Sep. Purif. Technol.* 227, 115715. doi:10.1016/j.seppur.2019.115715

Xu, X., Zhang, W., Hu, Y., Wang, Y., Lu, L., and Wang, S. (2017). Preparation and overall energy performance assessment of wide waveband two-component transparent NIR shielding coatings. *Sol. Energy Mater. Sol. C* 168, 119–129. doi:10.1016/j.solmat.2017.04.032

Yang, Z., Zhang, M., Zhao, X., Hu, R., Zhao, H., Zeb, S., et al. (2024). Fluorine-doped ATO NCs with enhanced LSPR effect for smart windows with adaptive solar modulation. *Ceram. Int.* 50 (11), 19543–19551. doi:10.1016/j.ceramint.2024.03.063

Yuan, H., Li, T., Wang, Y., Ma, P., Du, M., Liu, T., et al. (2020). Photoprotective and multifunctional polymer film with excellent near-infrared and UV shielding properties. *Compos. Commun.* 22, 100443. doi:10.1016/j.coco.2020.100443

Zhang, Z., Ma, H., He, Y., Shi, B., Zhong, J., Zhou, Y., et al. (2024). High reflectivity and latent heat synergetic TiO2/Cs0.33WO3-PU double-layer materials with zero transmittance. *Chem. Eng. J.* 496, 154104. doi:10.1016/j.cej.2024.154104